Dalton Transactions

Identification and Characterization of the Intermediate Phase in Hybrid Organic–Inorganic MAPbI3 Perovskite

Journal:	*Dalton Transactions*
Manuscript ID	DT-ART-11-2015-004420.R1
Article Type:	Paper
Date Submitted by the Author:	05-Jan-2016

Complete List of Authors:	Guo, Xin; Case Western Reserve University, Materials Science and Engineering McCleese, Christopher; Case Western Reserve University, Kolodziej, Charles; Case Western Reserve University, Chemistry Samia, Anna Cristina; Case Western Reserve University, Chemistry Zhao, Yixin; Shanghai Jiao Tong Univeristy, School of Environmental Science and Engineering Burda, Clemens; Case Western Reserve University, Chemistry

Journal Name

ARTICLE

Identification and Characterization of the Intermediate Phase in Hybrid Organic–Inorganic $MAPbI_3$ Perovskite

Received 00th January 20xx,
Accepted 00th January 20xx

DOI: 10.1039/x0xx00000x

www.rsc.org/

Xin Guo,[a,b] Christopher McCleese,[b] Charles Kolodziej,[b] Anna C. S. Samia,*[,b] Yixin Zhao*[,c] and Clemens Burda*[,a,b]

Perovskite films were prepared using single step solution deposition at different annealing temperatures and annealing times. The crystal structure, phases and grain size were investigated with XRD, XPS and SEM/EDX. The prepared films show a typical orientation of tetragonal perovskite phase and a gradual transition at room temperature from the yellow intermediate phase to the black perovskite phase. Films with high purity were obtained by sintering at 100 °C. In addition, the chemical composition and crystal struture of intermediate phase were investigated in detail. FTIR, UV-vis and NMR spectra revealed the occurance of DMF complexes. Interestingly, the intermediate phase could be transformed to the black perovskite phase upon X-ray irradiation. In addition, the recovery of the aged perovskite films from a yellow intermediate phase back to the black perovskite was shown to be viable via heating and X-ray irradiation.

1. INTRODUCTION

Recently, organic–inorganic hybrid semiconductor materials with perovskite structure have attracted attention as light sensitizers for solar cells due to their superb photovoltaic characteristics [1-3]. This class of materials is advantageous for solar cell applications particularly with respect to their relatively low processing cost and high energy conversion efficiencies [4-6], with a certified power conversion efficiency (PCE) of 20.1% reported in 2014 by Seok et al. [7]. These organic–inorganic hybrid semiconductors can be fabricated from relatively inexpensive materials by a simple solution process with low annealing temperatures and their cost can be reduced with mass production [8-11]. Moreover, solar cells based on these compounds possess several advantages such as excellent optical properties with a wide range of light absorption that is tunable by managing the chemical composition, ambipolar charge transport, high charge carrier mobility and long electron-hole diffusion lengths [12-16]. These perovskites are easy to process and can be versatile alternative light absorbers for solar cell applications.

Organic–inorganic hybrid perovskites are metal-halide-based semiconductors with the general formula (RNH_3) MX_3 (R = C_nH_{2n+1}; X = halogen I, Br, Cl; M = Pb, Sn, Ge etc.) [17-22] and they can have diverse structures. At high temperature, they have a cubic perovskite structure (space group $Pm\bar{3}m$), which can be represented by the simple building block ABX_3, where B is the metal cation and X is a halide anion [23, 24]. This unique combination makes transitions to different space groups and different properties possible. The methylammonium ion, $CH_3NH_3^+$ (MA), located in a cage surrounded by four PbI_6 octahedra, can move conditionally inside the cage [24]. The spacing between the inorganic layers can vary according to the occupation and orientation of the organic cations [24, 25]. With decreasing temperature, the perovskite undergoes two phase transitions along with reorientation motions of MA, which can be detected by variable temperature NMR [26, 27]. The first phase change from cubic to tetragonal occurs at approximately T_c = 330.4 K with decreased disordered states of the MA cation [27]. The space group of the tetragonal phase is confirmed to be *I4/mcm* [27], as shown in **Figure 1A**. When the temperature is further lowered, the organic cations become more localized and the tetragonal phase changes to an orthorhombic structure with space group *Pnma* at T_c = 161.4 K, as shown in **Figure 1B**. Single crystal X-ray diffraction revealed that with decreasing temperature the rotation angle of the octahedra also increased monotonically [28]. All these structural changes have a close correlation to the temperature

[a] Department of Materials Science and Engineering, Case Western Reserve University, 10900 Euclid Avenue, Cleveland, Ohio 44106, United States.
[b] Department of Chemistry, Case Western Reserve University, 10900 Euclid Avenue, Cleveland, Ohio 44106, United States.
[c] School of Environmental Science and Engineering, Shanghai Jiao Tong University, 800 Dongchuan Rd., Shanghai 200240, China.
E-mail: anna.samia@case.edu; yixin.zhao@sjtu.edu.cn; burda@case.edu;

† Electronic Supplementary Information (ESI) available: The calculated XRD data using the Jade MDI. The average grain size calculated in Halder-Wagner method by Rigaku PDXL. The lattice parameters of crystal structure for intermediate phase estimated using pattern indexing in MDI jade. The SEM images and EDX spectra of the sample after XPS. See DOI: 10.1039/x0xx00000x

suggesting a direct effect on the microstructures formed by annealing under different conditions.

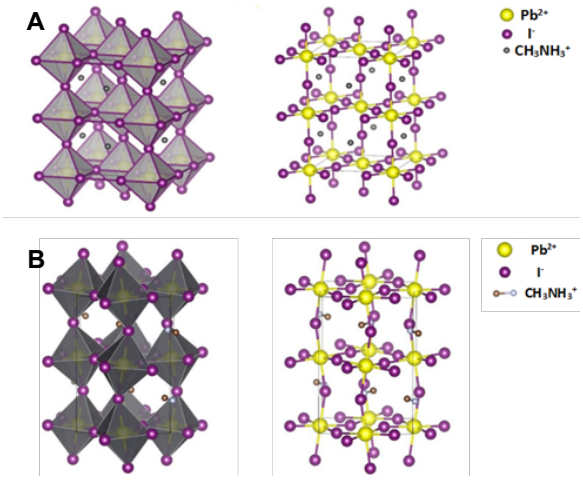

Fig. 1 Schematic of A) the tetragonal perovskite $CH_3NH_3PbI_3$ and B) the orthorhombic perovskite $CH_3NH_3PbI_3$.

The effect of the annealing temperature on the preparation of mixed halide perovskite films prepared using the spin coating technique was studied by Grätzel and Snaith et al. [29, 30, 31]. For solution processed perovskites, the formation of perovskite could occur in the temperature range of 40-160°C [7]. Grätzel et al. [29] reported that annealing at 100 °C would effectively reduce the time required for the complete conversion of final perovskite film resulting in a uniform black material with a stable absorption profile. The samples annealed at temperatures lower than 100 °C exhibited additional absorption shoulders at lower wavelengths while the samples annealed at 100 °C showed the highest absorption above the band gap energy. With increasing annealing temperature (> 100 °C), despite a much faster conversion of perovskite crystals (almost instantaneously at T > 150 °C), not only did the absorption decrease but also the additional absorption of PbI_2 at 500 nm appeared indicating the decomposition of the perovskite [29]. The structural and optical properties of the perovskite prepared in a range of compositions at temperatures from 40 to 190 °C for 30 min in a dry nitrogen atmosphere have been investigated [32]. Experiments confirmed that 30 min was sufficient to complete the reaction in the $CH_3NH_3PbI_3$ ($MAPbI_3$) thin films and at temperatures higher than 150°C, methylammonium iodide (MAI) vapor escaped from the film [32].

In this work, the $CH_3NH_3PbI_3$ perovskite films prepared by solvent evaporation under reduced pressure (12.7 torr) at a range of temperatures around the transition point T≈ 54-57 °C [27] were examined. The formation of intermediate phase of PbI_2-MAI-DMF (*N,N*-Dimethylformamide) was also reported. Jen et al. [33] have reported that different intermediates can be involved in the perovskite film preparation via different processing routes, which govern film evolution and morphology of the final microstructures. Seok et al. [12] have brought forward the formation of intermediate phase of PbI_2-MAI-DMSO and obtained extremely uniform and flat perovskite films via an intermediate film. However, there is limited information on the phase transformation of perovskite from DMF solvent. We propose that the intermediate phase comes from the intercalation process of the $CH_3NH_3^+$ into the inorganic cage during the solvent evaporation. We also define the conditions at which an intermediate phase would be expected, and how it can be traced with X-ray diffraction (XRD) and X-Ray photoelectron spectroscopy (XPS) analysis. In addition, the XRD analysis confirmed that phase degradation is reversible and degraded perovskite can be recovered.

2. EXPERIMENTAL SECTION

2.1. Materials. Commercial PbI_2 powder (99%, Sigma-Aldrich) and DMF solvent (99.8%, Sigma-Aldrich) were used as received. Methylammonium idodide powder was synthesized by reacting hydroiodic acid (57 wt%, Sigma-Aldrich) with methylamine (33 wt% in methanol, Sigma-Aldrich) in an ice bath for 2 h with stirring. The mixture was dried at 65 °C for 30 min using a rotary evaporator. The precipitant obtained was washed three times with diethyl ether and dried in a vacuum oven at 60 °C for 24 h.

2.2. Synthesis of $MAPbI_3$ and complexes. $MAPbI_3$ perovskite films were prepared by drop casting a 25 wt % mixture of PbI_2 and MAI with a molar ratio of 1:1 dissolved in *N,N*-Dimethylformamide. $MAPbI_3$ perovskite films were heated at temperatures from 40-80°C and 100°C at time intervals 15 min, 30 min, 45 min, 60 min on a glass substrate to evaporate the DMF solvent. 461 mg of PbI_2 and 160 mg MAI were dissolved in 1 ml of DMF to prepare the 1M perovskite precursor solution. 1M precursor solution of PbI_2 in DMF was used as a control. The precursor was drop-casted onto a glass substrate and dried under reduced pressure (12.7 torr) to form a complex, which was used for infrared (IR) spectroscopy and UV-Vis absorption measurement. Both precursors were used for UV-vis spectroscopic study.

2.3. Materials Characterization. X-ray diffraction patterns were obtained using a Rigaku MiniFlex instrument Cu Kα beam (λ= 1.54 Å). Surface composition analysis was performed using PHI Versaprobe 5000 Scanning X-Ray Photoelectron Spectrometer with a Al Kα beam (λ= 8.34 Å). The monochromatic Al Kα radiation (1486.6eV) was used to excite photoelectrons under ultra-high vacuum. 500 MHz Bruker Ascend Avance III HD Spectroscopy was used for Nuclear Magnetic Resonance (NMR) analysis. A Thermo Nicolet NEXUS 870 FT-IR spectrometer was used to collect the FT-IR spectral data for DMF (liquid phase), PbI_2-DMF complex, PbI_2-MAI-DMF complex and $MAPbI_3$ in the 600 cm^{-1} - 4000 cm^{-1} range. The UV-visible spectrum was recorded on a Cary 50 Bio UV-visible spectrophotometer. Scanning electron microscopy (SEM) images and energy-dispersive X-ray spectroscopy (EDX) spectra were acquired with a Phenom ProX.

3. RESULTS AND DISCUSSION

3.1. Effect of Heat Treatment

The synthesis of hybrid halide perovskite was first carried out by sintering at 70 °C for 15, 30, 45, and 60 min. The XRD patterns of 4 different samples were labeled for comparison with the calculated XRD data using MDI Jade software (see **Table S1-S2**), and the results are shown in **Figure 2**.

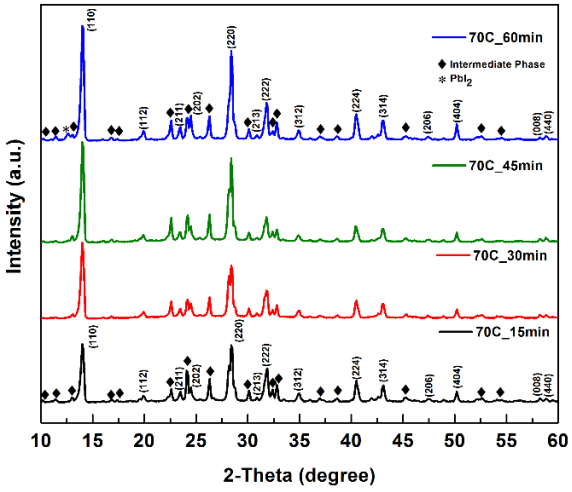

Fig 2. XRD patterns of perovskite films prepared at 70 °C for 15, 30, 45, and 60 min at 12.7 torr. In all cases the intermediate phase is still present.

The typical peaks at 14.10°, 23.47°, 28.42°, 30.89° correspond to (110), (211), (220), (213) of the tetragonal phase perovskite, and are shown respectively. There are unidentified peaks at 10.24°, 11.42°, 13.01°, 16.80°, etc. (indicated by black diamonds in Figure 2). The unidentified peaks did not match either the pure PbI_2 or MAI tetragonal phase, which was stable at room temperature. This suggested that hitherto there has existed a not well described intermediate phase, which might be a complex of PbI_2-DMF, complex of PbI_2-MAI-DMF, or hydrate compound $(CH_3NH_3)_4PbI_6{\cdot}2H_2O$ [34]. With increasing annealing time at 70 °C, the intensity of intermediate phase peaks did not change significantly, indicating that a stable intermediate phase existed at this temperature.

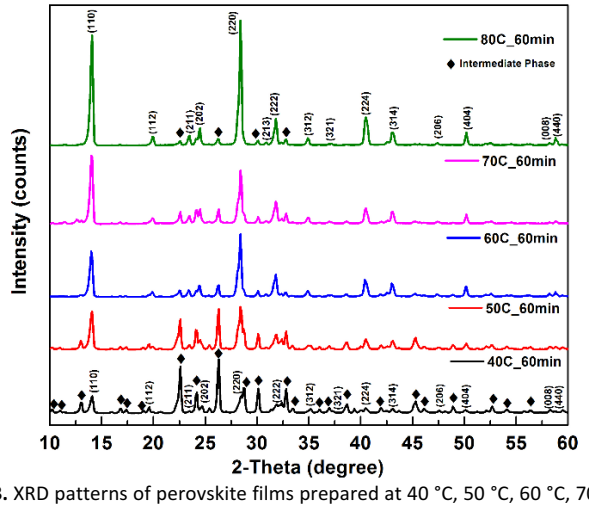

Fig 3. XRD patterns of perovskite films prepared at 40 °C, 50 °C, 60 °C, 70 °C, 80 °C for 60 min at 12.7 torr. Increased sintering temperatures led to increased perovskite purity.

In order to investigate the effect of heat treatment at different temperatures, a second set of experiments was conducted at 40 °C, 50 °C, 60 °C, 70 °C, and 80 °C for 60 min. The indexed XRD patterns of the 5 samples prepared at different temperatures are shown in **Figure 3**. With increasing temperature, the peaks of the intermediate phase decreased implying that a purer perovskite film was obtained. In addition to perovskite and the intermediate phase, the prepared films also produced a preferential orientation of (110) and (220) planes.

The average grain size was estimated using the Halder-Wagner method (see **Table S5**). With increasing annealing time at 70 °C, the mean grain size tended to increase. Grain size of the samples annealed at increasing temperatures only showed an increasing trend on the whole except for an anomaly for the samples heated at 50 °C, possibly due to abnormal grain growth with the phase transition occurring during the annealing process. At a temperature close to the transition point, the energetically more favored cubic phases nucleate at the grain boundary of the tetragonal matrix and the lattice distortion is induced by incoherent interfaces between these two phases. This distortion provides an additional driving force for secondary grains to grow abnormally at the expense of neighboring grains. At temperatures higher than 330 K, the phase transformation has nearly gone to completion and the observed continuous grain growth in the single cubic phase region is mainly driven by a higher thermally activated nucleation rate and diffusion-facilitated migration of the grain boundaries. The continued grain growth at higher temperatures also promotes the growing along the preferentially oriented direction <110> and generates non-spherical grain shapes such as wires, polyhedron or dendrite structures. The sharper and more symmetric XRD peaks obtained with increasing temperatures also indicate a better crystallinity of grains with less defects. Furthermore, the higher evaporation rate of solvent and enhanced transformation from the metastable intermediate phase offers resources for further grain nucleation and growth at increasing temperatures.

3.2. Intermediate Phase Investigations

The perovskite film prepared at 70 °C was investigated with a shorter heating time of 10 min in order to observe the intermediate phase. A portion of the film stayed yellow after sintering under vacuum (12.7 torr) which was the intermediate phase and gradually turned black after being placed into a desiccator at room temperature for several hours as shown in **Figure 4**. The XRD patterns of the sample before and after 4hrs storage are also shown in **Figure 4A and 4B**. The peaks with increasing intensity are located at 14.01°, 19.6°, 28.66°, 30.12°, 31.78°, 32.78°, 45.25° which agree well with the tetragonal perovskite phase. Peaks with decreasing intensity are located at 10.24°, 11.42 °, 13.01°, 22.56°, 24.12°, 26.26° which correlate with the observation of the intermediate yellow phase. By a comparison with the calculated XRD data of PbI_2-DMF complex and $(CH_3NH_3)_4PbI_6{\cdot}2H_2O$ (**Table S3-S4**), there is a typical peak at 13.01° that is not present in the PbI_2-DMF or the hydrated complex. This implies a high possibility of an intermediate phase of PbI_2-MAI-DMF complex. A sample of PbI_2-DMF complex was prepared for comparison and the XRD pattern shown in **Figure S3** gives a clear difference between the PbI_2-DMF complex and the intermediate phase. After ruling out the perovskite peaks, the spectrum can be identified as a monoclinic structure (See **Table S6**).

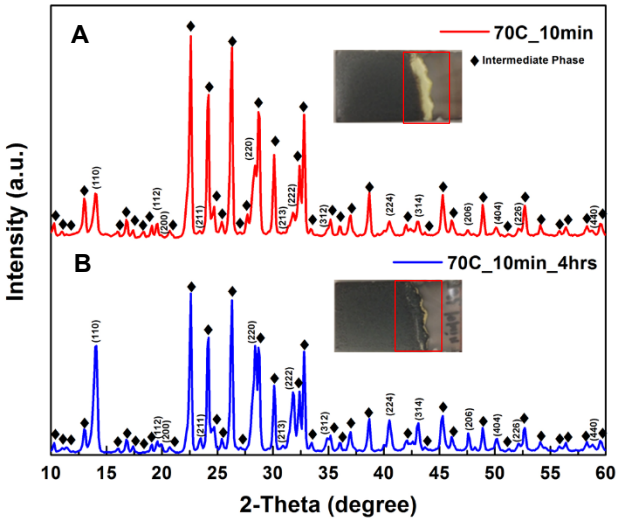

Fig 4. XRD patterns of perovskite films A) heated at 70 °C for 10 min (red) and B) 4 hrs after the heating took place (blue), showing continued transformation of intermediate phase into tetragonal perovskite. The insets show photographs of the corresponding samples.

The intermediate phase was apparent in the perovskite films sintered in the temperature range between 40 and 80 °C implying that the intermediate phase was both thermodynamically and kinetically metastable. It was also found that the sample annealed at room temperature for 30 min under reduced pressure (12.7 torr) was composed of intermediate phase in **Figure S3**. Comparing this sample with the XRD pattern of the sample annealed at 70°C for 10 min under 12.7 torr, the intermediate phases in both samples have almost the same pattern except for different peak intensities due to different orientations. The pure intermediate phase is hardly seen due to the transformation into perovskite during the XRD measurement.

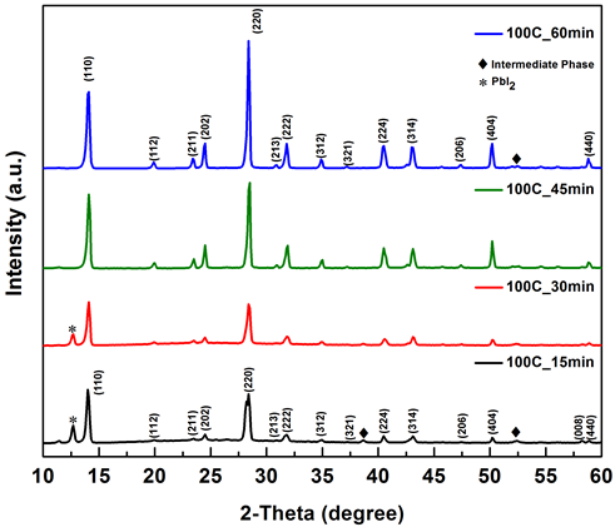

Fig 5. XRD patterns of perovskite films prepared at 100 °C at 4 durations of 15, 30, 45, 60 min at 12.7 torr, indicating almost complete transformation into tetragonal perovskite with high purity.

In order to obtain the perovskite with a higher purity, the synthesis conditions under which the intermediate phase can undergo a complete transition to the perovskite need to be investigated. Consequently, the heat treatment at 100 °C in four different time scales 15, 30, 45, 60 min were explored. The XRD patterns of samples, prepared at 100 °C at 4 different durations are shown in **Figure 5** and are labeled for comparison with the calculated diffraction patterns of perovskite phases.

The samples heated for 15 and 30 min showed a common peak at 12.6° indicating the existence of PbI_2 resulting from the decomposition of the intermediate phase which itself might be a complex of PbI_2-MAI-DMF. The perovskite films prepared at 100 °C had a higher purity. The intermediate phase converted almost completely into the perovskite at this temperature and there was very little intermediate phase left as shown from the XRD data. A preferred orientation along the (110) direction was observed in the samples prepared at 100 °C and the longer heating times positively impact the formation of oriented perovskite film.

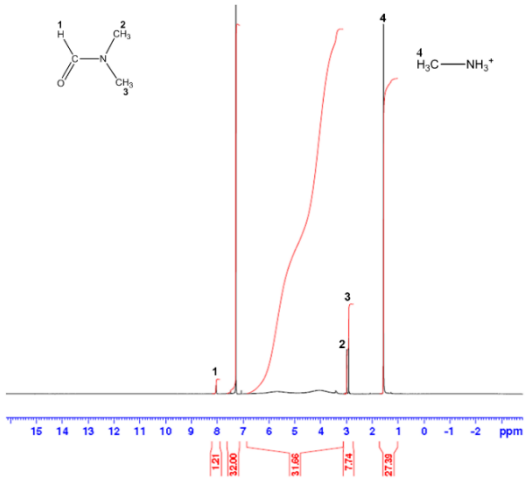

Fig 6. The ^{1}H NMR spectrum of sample annealed at 100°C for 60 min. The chemical shift of peak 1 at 8.02 ppm, peak 2 at 2.96 ppm and peak 3 at 2.89 ppm corresponding to the different types of protons in DMF as labeled. Peak 4 at 1.54 ppm and peak at 7.26 ppm result from the proton of the MA group in the perovskite and deuterated chloroform, respectively.

To verify the existence of DMF in the intermediate phase, powders from the sample annealed at 100 °C for 60 min was used for ^{1}H NMR analysis shown in **Figure 6**. The chemical shift of peaks at 8.02 ppm, 2.96 ppm and 2.89 ppm confirmed the presence of DMF. Although the bulk perovskite powders remain insoluble in chloroform, a small amount of MA and DMF molecules from intermediate phase can be dissolved. By comparing the integrated peak intensities, the ratio of residual DMF to dissolved MA molecules is around 1:7.5. This confirmed that a small amount of DMF from the intermediate phase existed in the purer sample annealed at 100°C, and thus also resides in samples with intermediate phase annealed at lower temperature or at short annealing times.

The composition of the intermediate phase was then investigated, and the sample prepared at 70 °C for 10 min was measured by X-ray photoelectron spectroscopy. The XPS survey spectra from the yellow intermediate region and the center dark region are shown in **Figure 7A**. The XPS spectrum showed that the chemical composition of both yellow color region and black color region of the perovskite film contained the same elements C, N, I, Pb, O but in different amounts. The yellow intermediate phase had a higher amount of carbon and oxygen than the black phase. By an analysis

of atomic concentrations from the peak area and relative sensitivity factor (R.S.F.) in table S7, the intermediate phase was comprised of 55.9% C 1s, 17.4% I 3d5, 9.7% O 1s, 9.4% Pb 4f, 7.6% N 1s while the black phase was composed of 39.0% I 3d5, 27.3% C 1s, 16.8% N 1s, 15.0% Pb 4f, 1.9% O 1s. The higher amount of oxygen and carbon in the intermediate phase may arise from the DMF (C_3H_7NO) forming a complex with MAI-PbI_2 rather than $(CH_3NH_3)_4PbI_6{\cdot}2H_2O$ since the spectrum of O 1s for intermediate phase showed two deconvoluted peaks at binding energies of 532.0 eV and 531.0 eV which were similar to the binding energy of C-O and Pb-O and were different from the binding energy O 1s (532.5-532.8 eV) in H_2O molecules or hydrates. It is possible that partial surface degradation occurred during the XPS measurement, the concentration of N and I was reduced as the decomposition of MAI into NH_3 vapor with C leftover and sublimation of I_2 from the iodide [35]. The composition of PbI_2-MAI-DMF complex could be determined roughly as $PbI_2{\cdot}3MAI{\cdot}DMF$ or $PbI_2{\cdot}MAI{\cdot}2MA{\cdot}DMF$ based on the concentrations of elements Pb, O and C (Pb: O: C=1: 1.03: 5.95) if the carbon leftover was simply from MAI. There could also be a small amount of intermediate phase in the dark sample region leading to minor oxygen content shown in **Figure 7B**, or simply surface hydroxyl groups. However, there is a higher possibility that the residual oxygen was from the DMF since there were residual C 1s peaks from DMF and the sample was under ultra-high vacuum in the XPS chamber. In addition, the atomic ratio in the dark phase is C: N: Pb: I =1.22: 0.99: 1.00: 2.60, which is closer to the $CH_3NH_3PbI_3$ ratio after excluding the excess carbon and nitrogen from the DMF which have a ratio to oxygen 3:1 and 1:1 respectively.

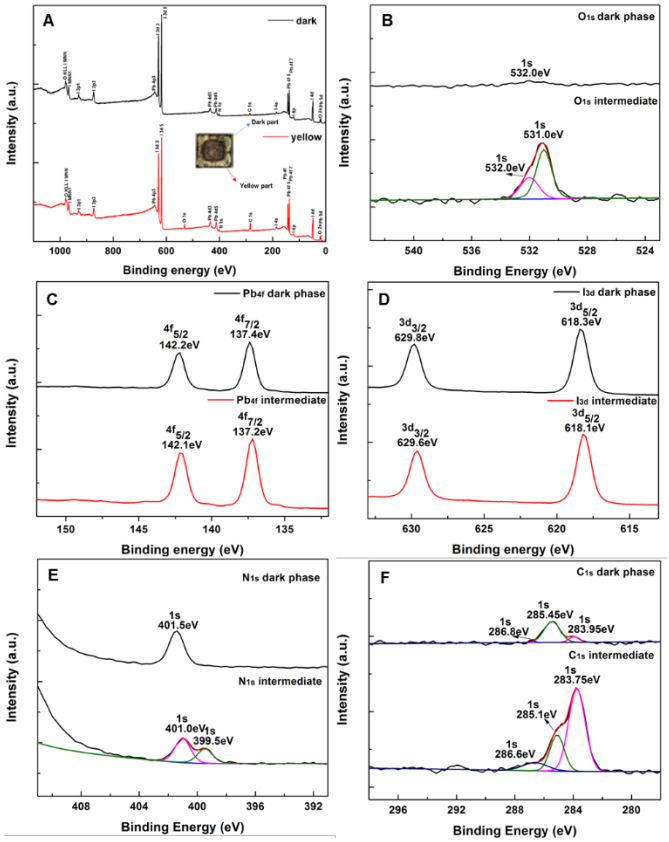

Fig 7. (A) XPS survey spectra of the sample prepared at 70 °C for 10 min after XRD exposure. Inset shows the photograph of the corresponding regions of yellow intermediate phase (red) and the center black phase (dark). XPS spectrum of the yellow intermediate phase (red) and the black phase (black) B) in the energy range of the O 1s binding energy; C) Pb 4f binding energy; D) I 3d binding energy; E) N 1s binding energy; F) C 1s binding energy.

The binding energy of Pb 4f in the intermediate phase (137.2 eV) is also smaller than the binding energy of Pb 4f in the pure PbO with a value 137.8 eV. This implied that it would not be pure PbO. Besides, the single maxima of symmetric Pb 4f peaks suggested that only one major Pb valence state existed in the intermediate phase eliminating the formation of PbO which could be converted from PbI_2 at high temperature. A pair of two faint peaks at 140.3 eV and 135.4 eV respectively next to the major peak pair indicated the existence of the bridge O-Pb bond between the PbI_2 and DMF. The binding energy of Pb 4f in the dark phase showed a 0.2 eV up-shift, indicating a stronger oxidized state of Pb after converting into a high symmetry tetragonal perovskite from the monoclinic complex. Correspondingly, the binding energy of I 3d in the intermediate phase (618.1 eV) with a relaxed structure was 0.2 eV smaller than in the dark phase (618.3 eV) with a close-packed structure. However, both of them had a binding energy smaller than I 3d in the PbI_2 (619.5 eV) showing that the intercalation of organic cations weakened the bonding strength between Pb and I in the PbI_2 inorganic cage. The spectrum of the intermediate phase in the energy range of the N 1s in **Figure 7E** demonstrated that the nitrogen shows two peaks at 401.0 eV and 399.5 eV corresponding to two states of nitrogen in the methylamine and dimethylformamide respectively. While only a single peak appears in the spectrum of the dark phase at 401.5 eV indicating the state of nitrogen in $MAPbI_3$. The N 1s binding energy in amide is usually around 399.7eV. The spectra were calibrated using the binding energy of C 1s (284.6 eV) as a standard. According to the XPS data of $CH_3NH_3PbI_3$ perovskite reported by Gao et al. [35], the N 1s in their sample prepared by co-evaporation of PbI_2 and CH_3NH_3I had a binding energy of 401.81 eV. The different binding energies of N 1s in these samples come from different chemical environments formed by mixed phases or structural changes during the XPS scan, as suggested in the XRD patterns in **Figure S4**. The C 1s spectra can be fitted using three peaks by symmetric Gaussian-Lorentzian function. The lowest one at 283.75eV in the intermediate phase was assigned to H_3C-N bonding in DMF. The other two peaks at 285.1eV and 286.6eV can be assigned to C-N in MAI and C-O bonding in DMF. In the dark phase, all three peaks showed varied positions indicating the chemical environment change after conversion from intermediate to dark phase. The intensity of C 1s peaks of DMF decreased significantly. The two peaks at 283.95eV and 286.8eV from DMF with a 0.2 eV shift display the transition of DMF from coordinated state to detached state while the peak at 285.45 eV with a 0.35eV shift results from the state change of MA^+ from the relaxed PbI_2-MAI-DMF complex structure to the more ordered $MAPbI_3$ perovskite.

The XRD patterns of the sample before and after XPS measurements are shown in **Figure S4**. After the XPS measurement, the sample was transformed to the black perovskite phase due to the long X-ray exposure time (180 min). This result shows that upon X-ray irradiation, a transformation from the intermediate phase to the black perovskite phase occurs for the solid state ingredients. From the XRD patterns shown in **Figure 4** and **S4**, the peaks at the same positions were found but with different intensities. This might be due to different orientations of the intermediate phase formed during the solvent evaporation.

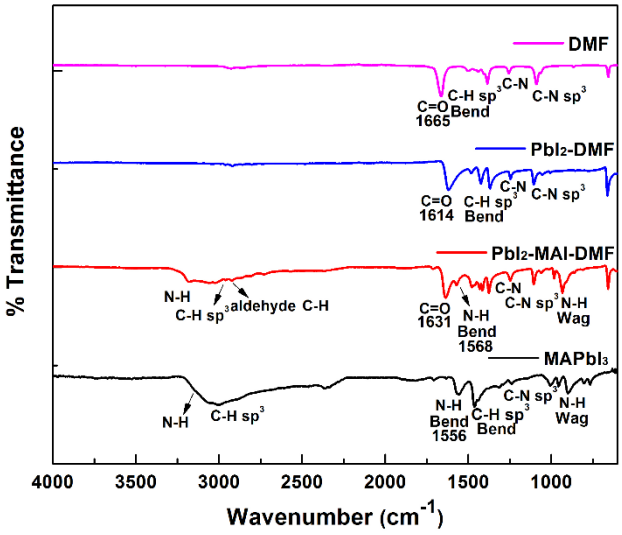

Fig 8. The FTIR spectrum of pure DMF (magenta), PbI_2-DMF complex (blue), PbI_2-MAI-DMF complex (red) and $MAPbI_3$ (black).

Confined interactions of DMF with PbI_2 as well as DMF with both PbI_2 and MAI were also verified by IR spectroscopy and the results are shown in **Figure 8**. The stretch vibration of the C=O bond appeared at 1665 cm^{-1} for the pure DMF, but shifted to lower wavenumber 1614 cm^{-1} for the PbI_2-DMF complex and 1631 cm^{-1} for PbI_2-MAI-DMF complex. It is expected that the C=O bond strength in the PbI_2-MAI-DMF complex should be decreased with MA^+ addition due to interaction with the Lewis acids MA^+ and Pb^{2+}. The addition of MAI weakens the interaction between DMF and PbI_2 by intercalation into a closer position to the PbI_2 framework. With the transformation of PbI_2-MAI-DMF complex to perovskite by annealing at 100 °C for 60 min, the C=O bond from DMF has almost disappeared and the N-H bond red shifts to a lower wavenumber suggesting stronger interaction with $[PbI_6]^{4-}$ in the compact $MAPbI_3$ perovskite lattice. It also shows that there was no O-H bond around 3500 cm^{-1} in both complexes suggesting no hydrated or adsorbed water existed while the N-H bond only appeared in the PbI_2-MAI-DMF complex.

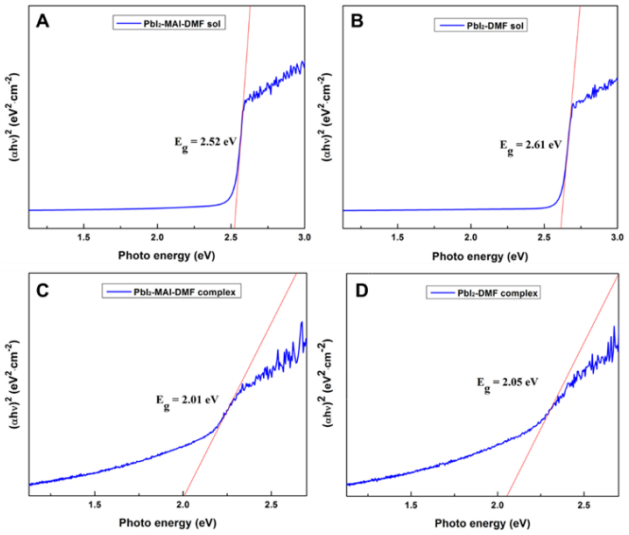

Fig 9. Tauc plots of optical absorption coefficient $(\alpha h\nu)^2$ vs. photon energy (hv) for (A) PbI_2-MAI-DMF solution, (B) PbI_2-DMF solution, (C) PbI_2-DMF complex and (D) PbI_2-MAI-DMF complex.

The differences between PbI_2-MAI-DMF complex and PbI_2-DMF complex can also be observed in the UV-vis spectrum of their solution and dry complex in **Figure S5**. When both were in the solution state, a sharp absorption manifested a well-ordered solvated structure formed by PbI_2 and DMF (slope=-0.1234) and by PbI_2, MAI, and DMF (slope=-0.1298) although the absorption onset red-shifted from 476 nm to longer wavelength 494.3 nm with the addition of MAI in the PbI_2-MAI-DMF solution. After drying, both crystalline complexes exhibited a plain absorption suggesting a broad distribution of density of states in the valence band (slope=-0.0152 for PbI_2-MAI-DMF complex and -0.0103 for PbI_2-DMF complex). The absorption onset of both complexes cannot be estimated directly due to a slightly rising slope of baseline. However, their optical band gap E_g can be determined from the extrapolation of the linear part of a Tauc plot in **Figure 9**. The bandgap values were 2.01eV for PbI_2-MAI-DMF and 2.05eV for PbI_2-DMF solid film complexes. The solvated complexes showed increased band gaps of 2.52eV and 2.61eV respectively. The lower band gap of the PbI_2-MAI-DMF complex versus the PbI_2-DMF complex is caused by interactions of MA^+ in the complexed structure.

4. Conclusions

We demonstrated that the perovskite film prepared at increasing temperatures had a preferential (110) orientation and increasing grain sizes. An intermediate phase was reported in the temperature range of 40 to 80 °C. At higher temperatures of ≥ 100 °C, the prepared films manifested a higher purity. The composition of the intermediate phase was investigated by XPS technique and the analysis of the spectra indicated the formation of PbI_2-MAI-DMF complex in the intermediate phase rather than the hydrate compound $(CH_3NH_3)_4PbI_6{\cdot}2H_2O$ and PbI_2-DMF complex. The FTIR spectra revealed the interaction of DMF with PbI_2 and DMF with both PbI_2 and MAI. The stretching vibration of C=O had a shift to lower wavenumber due to more interactions with Lewis acids Pb^{2+} and MA^+ for both PbI_2-DMF complex and PbI_2-MAI-DMF complex in comparison with pure DMF. The UV-vis spectra of both complexes shifted to a shorter wavelength when dried from the solution state to the crystalline state and the bandgap of PbI_2-DMF complex was further lowered with the additions of MA^+ in PbI_2-MAI-DMF complex. Surprisingly, the intermediate phase could be transformed to tetragonal perovskite phase under the exposure of X-rays as a new path of photo-irradiation induced synthesis of perovskites. A partial recovery of degraded perovskite film via intermediate phase was also demonstrated to be feasible. The DMF vapor can wet the degraded film and allow for a more uniform film by more evenly distributing the components. The sample undergoing different stages in line with the recovery protocol is shown in the **supporting information**.

Acknowledgements

We thank Dr. Prashansa Agrawal for the assistance with NMR measurement.

References

1 P. Gao, M. Grätzel and M. K. Nazeeruddin, *Energy Environ. Sci.*, 2014, **7**, 2448.
2 S. Chavhan, O. Miguel, H.-J. Grande, V. Gonzalez-Pedro, R. S. Sánchez, E. M. Barea, I. Mora-Seró and R. Tena-Zaera, *J. Mater. Chem. A*, 2014, **2**, 12754-12760.
3 Y. Zhao and K. J. Zhu, *Phys. Chem. Lett.* , 2013, **4**, 2880−2884.
4 J. H. Heo, S. H. Im, J. H. Noh, A. Sarkar, M. K. Nazeeruddin, M. Grätzel and S. Seok, *Nature Photonics*, 2013, **7**, 486–491.
5 L. Wang, C. McCleese, A. Kovalsky, Y. Zhao and C. Burda, *J. Am. Chem. Soc.*, 2014, **136 (35)**, pp 12205–12208.
6 Y. Zhao and K. Zhu, *J. Phys. Chem. Lett.*, 2014, **5**, 4175−4186.
7 N. J. Jeon, J. H. Noh, W. S. Yang, Y. C. Kim, S. Ryu, J. Seo and S. Seok, *Nature*, 2015, **517**, 476–480.
8 Z. Cheng and J. Lin, *Crystal Eng. Comm.*, 2010, **12**, 2646–2662.
9 Z. Ku, Y. Rong, M. Xu, T. Liu and H. Han, *Scientific Reports*, 2013, **3**, 3132.
10 L. Etgar, P. Gao, Z. Xue, Q. Peng, A. L. Chandiran, B. Liu, M. K. Nazeeruddin and M. Grätzel, *J. Am. Chem. Soc.*, 2012, **134 (42)**, pp 17396–17399.
11 Y. Zhao and K. Zhu, *J. Mater. Chem. A*, 2015, Advance Article.
12 N. J. Jeon, J. H. Noh, Y. C. Kim, W. S. Yang, S. C. Ryu and S. Seok, *Nature Materials*, 2014, **13**, 897–903.
13 Z. Zhu, J. Ma, Z. Wang, C, Mu, Z. Fan, L. Du, Y. Bai, L. Fan, H. Yan, D. L. Phillips and S. Yang, *J. Am. Chem. Soc.*, 2014, **136**, 3760−3763.
14 A. Marchioro, J. Teuscher, D. Friedrich, M. Kunst, R. van de Krol, T. Moehl, M. Grätzel, J.-E. Moser, *Nature Photonics*, 2014, **8**, 250–255.
15 P. Qin, S. Tanaka, S. Ito, N. Tetreault, K. Manabe, H. Nishino, M. K. Nazeeruddin and M. Grätzel, *Nature Communications*, 2014, **5**, 3834.
16 Y. Zhao, A. M. Nardes and K. Zhu, *J. Phys. Chem. Lett.*, 2014, **5**, 490−494.
17 N.-G. Park, *J. Phys. Chem. Lett.*, 2013, 4, 2423−2429.
18 K. Liang, D. B. Mitzi and M. T. Prikas, *Chem. Mater.*, 1998, **10**, 403-411.
19 R. Lindblad, D. Bi, B. W. Park, J. Oscarsson, M. Gorgoi, H. Siegbahn, M. Odelius, E. M. J. Johansson and H. Rensmo, *J. Phys. Chem. Lett.*, 2014, **5**, 648−653.
20 O. Malinkiewicz, A. Yella, Y. H. Lee, G. M. Espallargas and M. Grätzel, *Nature Photonics*, 2014, **8**, 128–132.
21 M. K. Nazeeruddin and H. J. Bolink, *J. Phys. Chem. Lett.*, 2013, **4**, 3623−3630.
22 J. Burschka, N. Pellet, S.-J. Moon, R. Humphry-Baker, P. Gao, M.K. Nazeeruddin and M. Grätzel, *Nature*, 2013, **499**, 316–319.
23 P. P. Boix, K. Nonomura, N. Mathews and S. G. Mhaisalkar, *Materials Today*, 2014, **Volume 17**, Number 1.
24 C. C. Stoumpos, C. D. Malliakas and M. G. Kanatzidis, *Inorg. Chem.*, 2013, **52**, 9019−9038.
25 Z. Chen, H. Li, Y. Tang, X. Huang, D. Ho and C. S. Lee, *Mater. Res. Express*, 2014, **1**,015034.
26 R. E. Wasylishen, O. Knop and J. B. Macdonald, *Solid State Communications*, 1985, **Vol.56**, No.7, pp.581-582.
27 T. Baikie, Y. Fang, J. M. Kadro, M. Schreyer, F. Wei, S. G. Mhaisalkar, M. Grätzel and T. J. White, *J. Mater. Chem. A*, 2013, **1**, 5628.
28 I. E. Castelli, J. M. Garcia-Lastra, K. S. Thygesen and K. W. Jacobsen, *APL MATERIALS*, 2014, **2**, 081514.
29 A. Dualeh, N. Tétreault, T. Moehl, P. Gao, M. K. Nazeeruddin and M. Grätzel, *Adv. Funct. Mater.* , 2014, **24**, 3250–3258.
30 M. Saliba, K. W. Tan, H. Sai, D.T. Moore, T. Scott, W. Zhang, L. A. Estroff, U. Wiesner and H. J. Snaith, *J. Phys. Chem. C* , 2014, **118**, 17171−17177.
31 G. E. Eperon, V. M. Burlakov, P. Docampo, A. Goriely and H. J. Snaith, *Adv. Funct. Mater.* , 2014, **24**, 151–157.
32 Z. Song, S. C. Watthage, A. B. Phillips, B. L. Tompkins, R. J. Ellingson and M. J. Heben, *Chem. Mater.*, 2015, **27**, 4612−4619.
33 S. T. Williams, C.-C. Chueh and A. K.-Y. Jen, *Small*, 2015, **11**, No. 26, 3088–3096.
34 B. R. Vincent, K. N. Robertson, T. S. Cameron and O. P. Knop, *Can. J. Chem.*, 1987, **65**, 1042.
35 Y. Li, X. Xu, C. Wang, C. Wang, F. Xie, J. Yang and Y. Gao, *J. Phys. Chem. C*, 2015, **119,** 23996–24002.

Table of Contents entry:

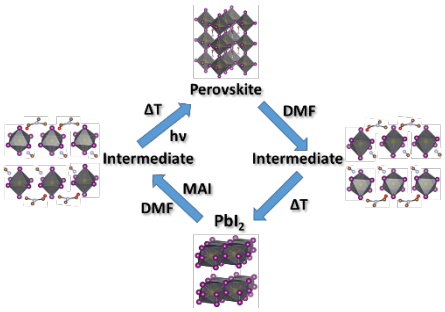

The intermediate phase bridges a reversible cycle between PbI_2 and high quality perovskite.